The Meteoritical Society

Meteoritics & Planetary Science 44, Nr 8, 1179–1191 (2009)
Abstract available online at http://meteoritics.org

Estimate of the magnetic field of Mars based on the magnetic characteristics of the Yamato 000593 nakhlite

Minoru FUNAKI[1*], Viktor HOFFMANN[2, 3], and Naoya IMAE[1]

[1]National Institute of Polar Research, 10-3, Midori-cho Tachikawa Tokyo 190-8518, Japan
[2]Institut für Geowissenschaften, Geophysik, Universität Tubingen, Sigwartstrasse 10, 72076 Tübingen, Germany
[3]Department für Geo- und Umweltwissenschaften, Universität München, Germany
[*]Corresponding author, E-mail: funaki@nipr.ac.jp

(Received 03 December 2008; revision accepted 13 July 2009)

Abstract–Yamato 000593, a nakhlite, was analyzed in terms of its magnetic record and magnetomineralogy. The natural remanent magnetization (NRM: 3.55–6.07 × 10^{-5} Am^2/kg) was thermally demagnetized at ~320 °C, and it was unstable against alternating field demagnetization. Based on analyses of thermomagnetic curves, the temperature dependence of hysteresis parameters, and microscopic observations, the magnetic minerals mainly consist of magnetite (0.68 wt% of the sample, including ~5% Fe_2TiO_4) of less than 100 μm in size, associated with minor amounts of monoclinic pyrrhotite (<0.069 wt% of the sample) and goethite. Thermal demagnetization of NRM at ~330 °C is explained due to an offset of magnetization of antipodal NRM components of magnetite, whereas it is not due to a pyrrhotite Curie point. Large magnetite grains show exsolution texture with ilmenite laths, and are cut by silicate (including goethite) veins that formed along cracks. Numerous single-domain (SD) and pseudo-single-domain (PSD) magnetite grains are scattered in the mesostasis and adjacent olivine grains. Moderate coercive forces of H_C = 6.8 mT and H_{RC} = 31.1 mT suggest that Yamato 000593 is fundamentally able to carry a stable NRM; however, NRM was found to be unstable. Accordingly, the meteorite was possibly crystallized at 1.3 Ga under an extremely weak or absent magnetic field, or was demagnetized by impact shock at 12 Ma (ejection age) on Mars. This finding differs from the results of previous paleomagnetic studies of SNC (shergottites, nakhlites, chassignites, and orthopyroxenite) Martian meteorites. The significant dipole magnetic field resulting from the molten metallic core was probably absent during the Amazonian Epoch (after 1.8 Ga) on Mars.

INTRODUCTION

Nakhlites are cumulus clinopyroxenites with minor olivine and mesostasis, probably originating from Mars (McSween 1985). The main opaque mineral phase within nakhlites is Ti-poor magnetite, which commonly contains ilmenite lamellae. If nakhlites should carry a significant natural remanent magnetization (NRM), this would contribute to analyses of the evolution of Mars, as it would indicate a dipole magnetic field resulting from a molten metallic core at the time of crystallization.

A large Martian meteorite weighing 13.7 kg, Yamato 000593 (Y-000593), was found on a bare ice field north of the JARE-IV nunataks in the Yamato Mountains, Queen Maud Land, Antarctica, by the 41st Japanese Antarctic Research Expedition (JARE) in 2000. The meteorite was classified as a nakhlite by Imae et al. (2003) based on the analyses of petrography, mineralogy, and noble gases. It consists of coarse-grained clinopyroxene (augite) associated with olivine and minor Ti-magnetite (Ti-poor) and iron sulfides. Antarctic meteorites are free of any type of artificial contamination, including magnetic contamination (e.g., by hand magnets), during collection and storage; therefore, we considered Y-000593 to be suitable for paleomagnetic analysis.

Shergottites, nakhlites, chassignites, and orthopyroxenite (the so-called SNC meteorites) may have formed by the remelting of a common mantle source region at different times (McSween 1997). Previous rock-based and/or paleomagnetic studies of SNC meteorites have sought to estimate the Martian crustal magnetic field when meteorites were crystallized. Consequently, many of the results revealed the weaker paleomagnetic field intensity less than 1/10 compared with the present Earth magnetic field (50 μT) or unclear of the field, when the SNC meteorites were cooled down from Curie point. For example, Cisowski (1986) reported that the magnetic behavior of the highly shocked

shergottites Shergotty, Zagami, and Elephant Moraine (EET) A79001 is likely to be single-domain (SD), while a multi-domain (MD)-like behavior was found for the low-shock nakhlites Nakhla and Governador Valadares. In the case of Shergotty, Cisowski reported paleofield intensities of between 0.25 and 2.0 μT for different temperature ranges, based on the ratio of NRM and thermal remanent magnetization (TRM) (Koenigsberger 1938; Thellier and Thellier 1959). Collinson (1986) reported stable but weak NRM values of 2.60–3.23 × 10^{-5} Am^2/kg for EETA79001 (basaltic shergottite) and 0.78–3.41 × 10^{-5} Am^2/kg for Allan Hills (ALH) A77005 (lherzolitic shergottite). These NRM values were considered to be carried by fine-grained magnetite or larger-grained titanomagnetite or pyrrhotite particles occurring at concentrations of less than 0.1 wt% of the sample. Collinson (1997) studied the magnetic properties of several Martian meteorites (Nakhla, Governador Valadares, Zagami, Lafayette, Chassigny, EETA79001, and ALH 84001), finding that the primary NRM component was acquired by TRM when the meteorites cooled from higher temperatures in the presence of a weak magnetic field of 0.5–5 μT. Shaw et al. (2001) estimated a paleointensity of 4 μT for Nakhla, using the microwave paleointensity technique. Rochette et al. (2001) reported the magnetic mineralogy of 10 SNC meteorites, revealing low Curie points of titanomagnetite for Nakhla (nakhlite), and Chassigny and Los Angeles (basaltic shergottites), and also for pyrrhotite in many other shergottites. Gattacceca and Rochette (2004) reported the magnetic field intensity in the range of 1–24 μT (mean 6.7 μT) from 14 different SNC meteorites using a REM (NRM/I_R; I_R: saturation isothermal remanent magnetization) technique. Kirschvink et al. (1997) reported that the stable NRM component in ALH 84001 was carried by pyrrhotite, implying a substantial magnetic field on Mars during its formation and primary cooling; however, the NRM directions were not parallel within the sample. To the contrary, the stronger paleomagnetic field was reported by Weiss et al. (2002) that a dipole-related magnetic field an order of magnitude stronger than the surface magnitude of the present-day Earth magnetic field, as estimated from the stable NRM of magnetite and pyrrhotite within ALH 84001. However, we should reconsider the variation of these field intensities due to the different crystallized ages or different experimental techniques (different intensities were obtained from the same meteorite).

SAMPLES

The surface of Y-000593 was originally covered by a black fusion crust and a thin greenish layer that appeared to represent the weathered products of the interior minerals. The rock was soft and brittle, and it was possible to remove selected grains from the bulk sample using a nail. Three samples (A, 0.8538 g; B, 0.5350 g; and C, 0.1445 g) were obtained from the interior material immediately below the greenish surface, extracted using a cold chisel made of nonmagnetic FeNi alloy (SUS304). The orientations of these samples relative to the original block were planned to be reconstructed based on photographs taken during the picking procedure; however, this approach failed in the case of samples B and C because of their fragile nature and featureless, disk-like shapes. Accordingly, the NRM of sample A was measured, and then it was immersed in epoxy resin and cut into three oriented sub-samples (A-1, A-2, and A-3) for NRM measurements. The individual weights of the sub-samples were likely to have been similar (based on their similar sizes), although they were not weighed because of the complications arising from the absorption of resin. Sample B was analyzed for thermal demagnetization, thermomagnetic curves, hysteresis properties, and other typical magnetic parameters. Sample C was immersed in resin to obtain a high-quality surface via polishing with diamond paste prior to polishing by silica colloid (0.1 μm diameter), in preparation for microscopic observations. The bulk volume of a piece of Y-000593 (0.1992 g) was measured to be 0.0907 ± 0.0017 cc by comparison with the volumes of the standard sample and Y-000593, using sand of zircon spheres (0.1 mm in diameter); accordingly, the bulk density was calculated to be 2.20 ± 0.04 g/cc. The grain density was measured to be 3.49 ± 0.04 g/cc by comparison with air pressure between the standard sample and Y-000593.

MAGNETIC PROPERTIES

NRM

NRM was measured using a 3-axis superconducting quantum interference device (SQUID) magnetometer with an attached 3-axis AF demagnetizer (2G Enterprise, 775R). The measurement error of each component seems to be less than 1%. The NRM intensities of samples A, B, and C were found to be relatively similar with values of 3.55 × 10^{-5}, 4.02 × 10^{-5}, and 6.07 × 10^{-5} Am^2/kg, respectively (Fig. 1). The intensities of the sub-samples could not be measured because of their unknown weights. The NRM direction of sample A showed an inclination (I) of 40° and declination (D) of 215°; however, the values obtained for sub-samples A-1, A-2, and A-3 showed a wide scatter, with a mean direction of (I = –53°, D = 113°), a precision parameter (K) of 6, and 95% confidence level (α_{95}) of 57°. The large difference in direction between sample A and the sub-samples probably reflects the effects of remagnetization during cutting of the sample.

AF and Thermal Demagnetization

Sub-sample A-3 was demagnetized by an AF field up to 100 mT in steps of 5 mT (Fig. 2). The curve of

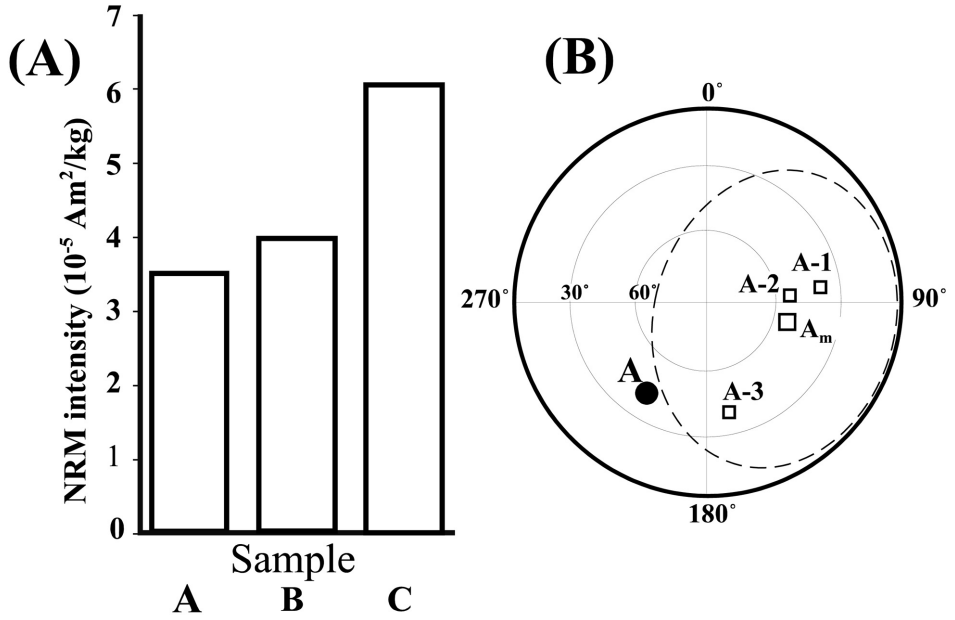

Fig. 1. (A): NRM intensity of samples A, B, and C. (B): NRM direction of sample A and sub-samples A-1, A-2, and A-3. Am: average direction of the sub-samples, ellipsoid: 95% probability.

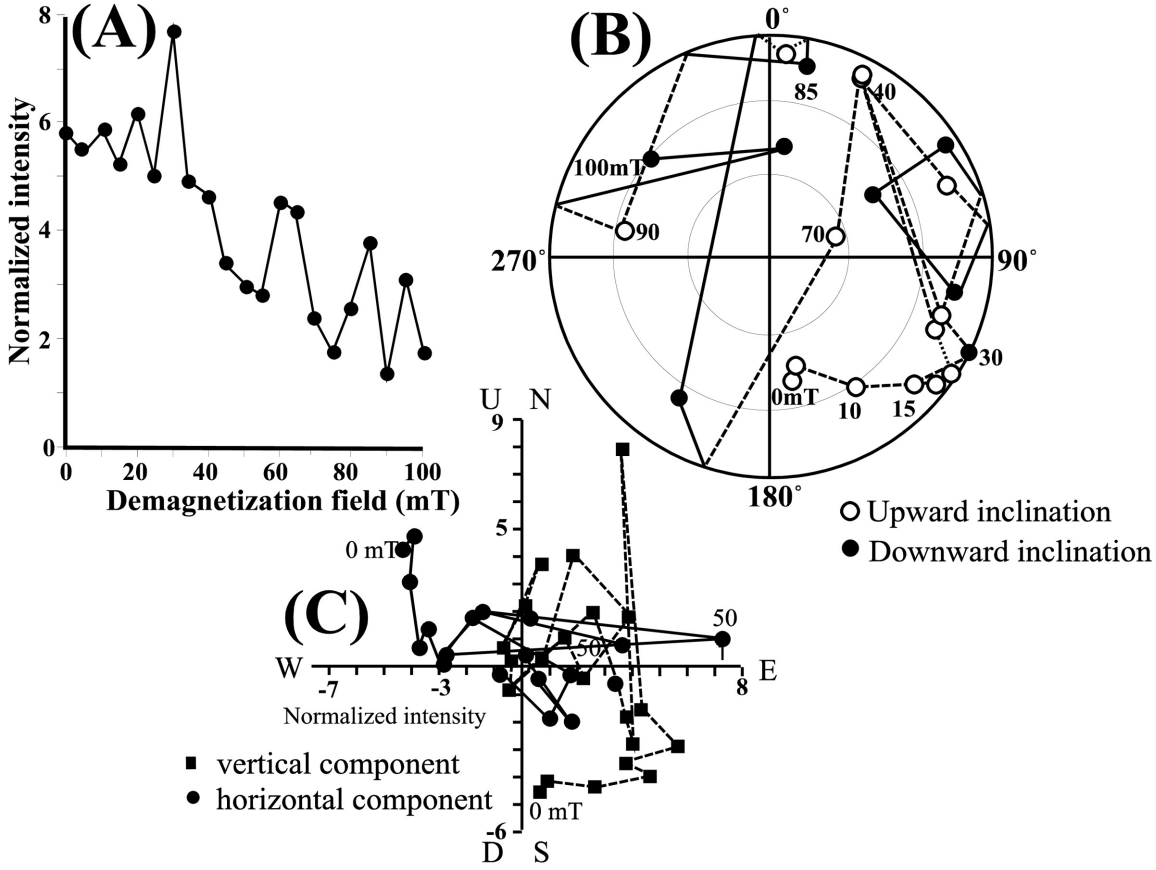

Fig. 2. AF demagnetization curves of NRM for sub-sample A-3. A) NRM intensity, B) NRM direction, and C) vector projection. Numbers in (B) and (C): demagnetization field intensity (mT).

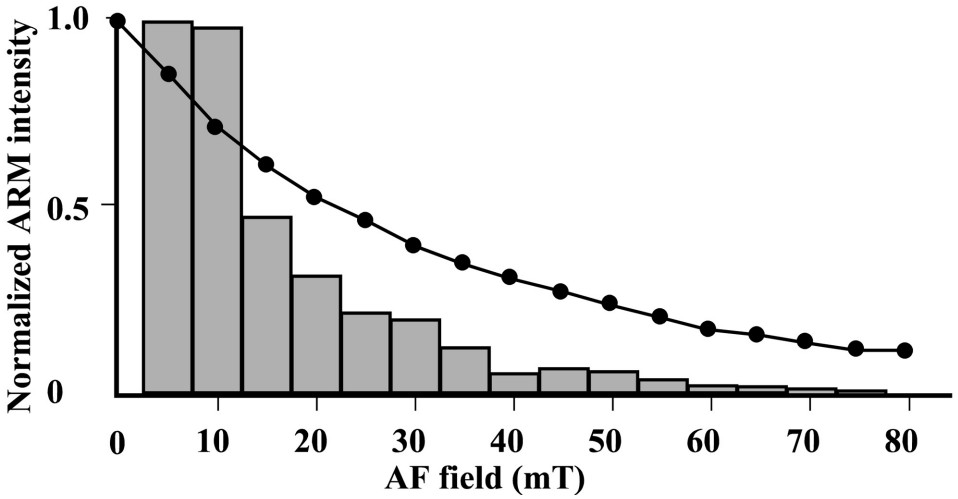

Fig. 3. AF demagnetization curve of ARM for sub-sample A-1 and its ARM coercivity spectra. ARM: h = 50 μT//+y and 80 mT of the alternating field.

demagnetization intensity shows a decreasing curve with irregular variations. The direction of NRM was highly unstable throughout demagnetization, although the variability was relatively minor between 15 and 30 mT. The obtained curves indicate that NRM is soft, without any hard component.

The sub-sample A-1 acquired an anhysteretic remanent magnetization (ARM) up to 80 mT under the steady magnetic field of 50 μT (h//+y), and then it was demagnetized by AF field up to 80 mT in steps of 5 mT, as shown in Fig. 3. The AF demagnetization curves of intensity gradually decreased up to 75 mT, and then it was almost flat up to 80 mT. The directions (ARM//+y) did not change throughout the demagnetization. Coercivity spectra of ARM obtained by the ARM demagnetization curve (Fig. 3) showed that the coercivity clearly distributes up to 55 mT, although the dominant spectra is <10 mT.

A chip of sample B was encapsulated in a silica tube under a vacuum of 10^{-3} Pa (without orientation) for measurement of the thermal demagnetization curve between 30 and 630 °C in steps of 50 °C (Fig. 4). The intensity (R = 2.80×10^{-5} Am^2/kg) decreased rapidly between 30 and 80 °C before decreasing gradually to almost zero at 330 °C. The curve is convex between 330 and 630 °C. The direction was relatively stable between 30 and 280 °C, but varied wildly between 280 and 630 °C. These curves indicate that NRM is demagnetized before 330 °C, with only an insignificant magnetization above 330 °C.

Thermomagnetic Curves

Thermomagnetic (Is–T) curves obtained for a small chip (0.0299 g) of sample B were measured from room temperature to 800 °C using a vibrating sample magnetometer (VSM) under an external magnetic field of 1.0 T, heating rate of 200 °C/h, and vacuum pressure of 10^{-4} Pa (Fig. 5). The noise level of VSM is guaranteed to less than 1% of the full scale of magnetization, and the temperature accuracy is 1 °C. As the sample is wrapped tightly in the fibriform silicon, the magnetic noise resulting from breaking up of the sample due to vibration is usually negligibly small. The curve obtained for the first run was irreversible, with a clearly defined Curie point (Tc) at 540 °C and a faint Tc at ~75 °C in the heating curve, with Tc = ~600 and ~320 °C in the cooling curve. The heating curve shows a slight convexity between 250 and 540 °C. The curve obtained for the second run was also irreversible, with the main Tc = ~600 °C and a minor Tc = ~320 °C during heating; a transition temperature of ~600 °C is recognized in the cooling curves.

The main Tc (= 540 °C) apparent in the heating curve of the first run corresponds to that of a low-Ti magnetite (~5% of Fe_2TiO_4; Akimoto 1962). This magnetite is consistent with the magnetite phase associated with the exsolution of ilmenite lamellae due to the high-temperature oxidation of titanomagnetite, as reported by Imae et al. (2003, 2005) and Mikouchi et al. (2003). The minor Tc (= 75 °C) apparent in the heating curve of the first run might represent the Curie point or phase-transition temperature of a goethite (α-FeO(OH)) phase formed due to weathering in the Antarctic ice sheet; however, we are currently unable to explain the magnetic minerals associated with the shift in the Curie point (or transition temperature) from Tc = 540 to 600 °C and with Tc (or transition temperature) = 320 °C in the second run.

Hysteresis Properties and Temperature Dependence

The saturation magnetization (I_S), I_R, coercive force (H_C), and remanent coercive force (H_{RC}) were obtained from the hysteresis loops using VSM generated by applying external magnetic fields of between +1.0 and −1.0 T at room temperature, before and after heating the sample to 800 °C (Table 1). The noise level of these values seems to be less than

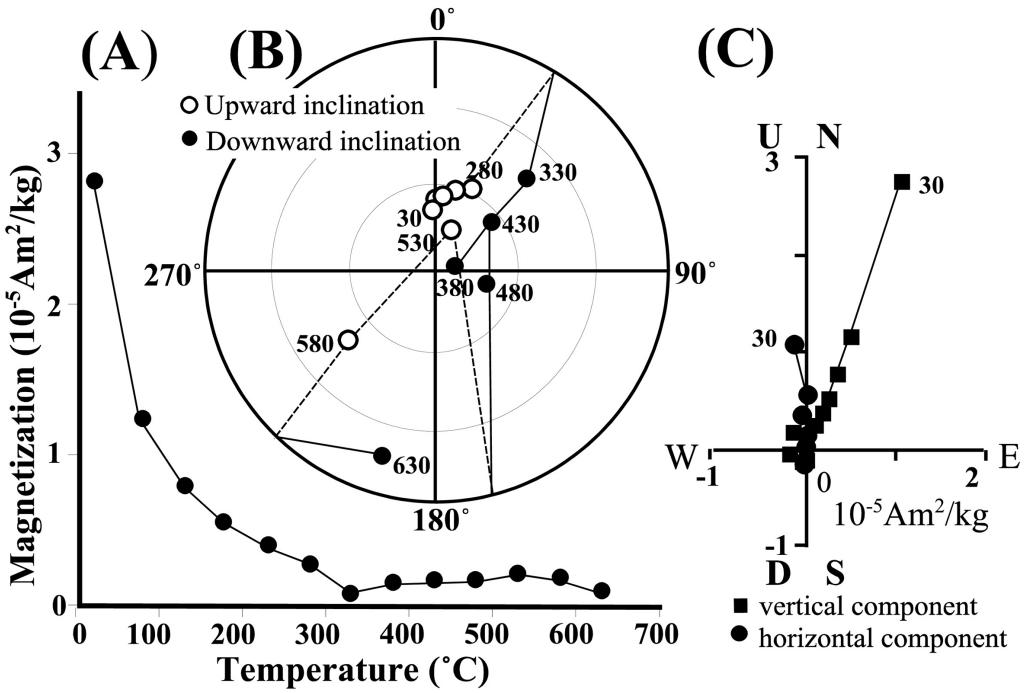

Fig. 4. Thermal demagnetization curves of NRM for a chip of sample B. A) NRM intensity, B) direction, C) vector projection. Numbers in (B) and (C): temperature of thermal demagnetization (°C).

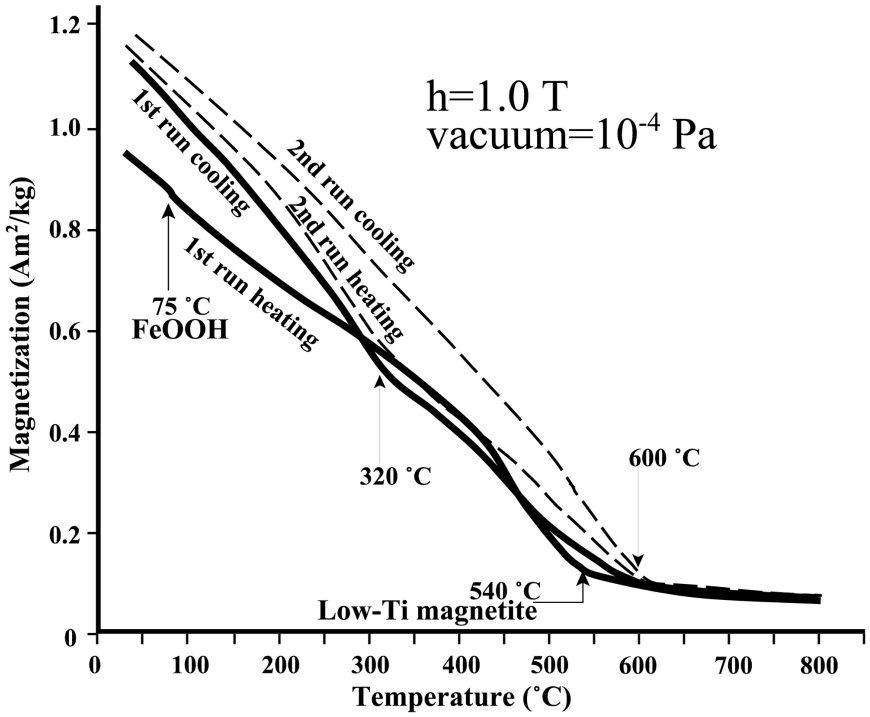

Fig. 5. Thermomagnetic curve of the first run (solid line) and the second run (dashed line) cycles. h: external magnetic field.

1% of the full scale. The original sample showed moderate values of H_C (6.8 mT) and H_{RC} (31.1 mT), indicating the ability to carry a stable NRM in the case of titanomagnetite, because these values belong to the range of SD and pseudo-single-domain (PSD; Day, 1977). After heating, the original values of I_S, I_R, H_C, and H_{RC} increased by factors of 1.6, 2.04, 3.1, and 4.6, respectively, suggesting the formation of fine-grained magnetic minerals during the heating process.

The temperature dependence of the hysteresis properties was measured under the same conditions as those used in

Table 1. Hysteresis properties of Y-000593 and other selected nakhlites.

Sample	NRM (10^{-5} Am^2/kg)	Stability	I_S (Am^2/kg)	IR (Am^2/kg)	H_C (mT)	H_{RC} (mT)	I_R/I_S	H_{RC}/H_C	Tc (°C)	REM	Reference
Y-000593	4.02	Unstable	0.640	0.0730	6.8	31.1	0.114	4.574	540	5.5×10^{-4}	This study
Heated to 800 °C	–	–	0.909	0.149	12.2	37.6	0.164	3.082	600	–	This study
Nakhla	7.92	–	0.237	0.0072	34	61	0.30	1.79	–	1.1×10^{-3}	Rochette et al. (2001)
Nakhla	1.3	Stable	–	–	40	62.5	0.2	1.56	150, 490	–	Cisowski (1986)
Gov. Valadares	5.1	Stable	–	–	42.5	575	0.26	1.35	–	–	Cisowski (1986)

NRM: natural remanent magnetization, I_S: saturation magnetization. I_R: saturation remanent magnetization, H_C: coercive force, H_{RC}: remanent coercive force, Tc: Curie point, and REM: ratio of NRM versus I_S.

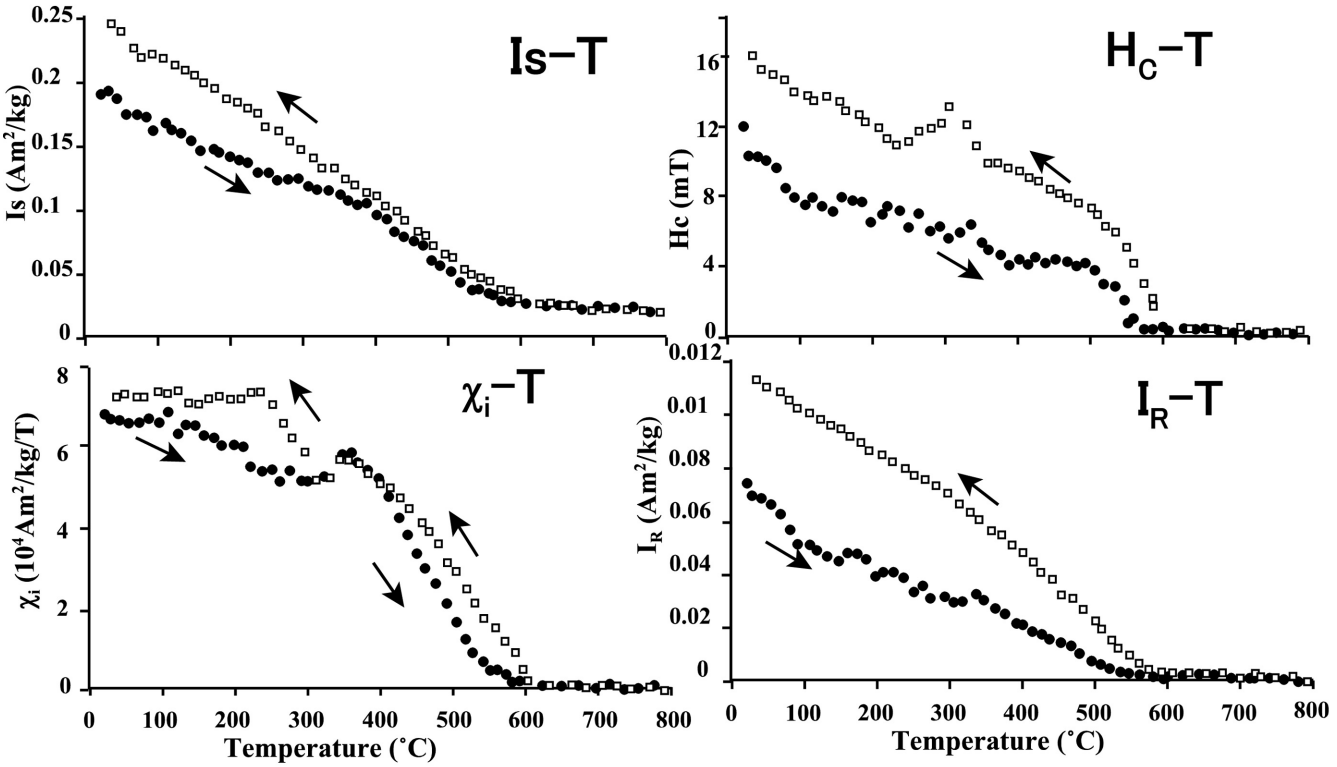

Fig. 6. Temperature dependence of saturation magnetization (I_S). coercive force (H_C), initial susceptibility (χ_i), and saturation isothermal remanent magnetization (I_R) values obtained in an external magnetic field of 1 T, vacuum of 10^{-4} Pa, and with a heating/cooling rate of 70 °C/h. Arrows: heating and cooling states

measuring the I_S–T curve, using the same VSM with a stepwise heating furnace and a different sample: measurements were performed in steps of 14 °C up to 800 °C, with heating and cooling rates of 70 °C/h. The curves showing the temperature-dependence of the magnetic parameters (I_S–T, I_R–T, H_C–T, and χ_i–T [χ_i: initial susceptibility]) were obtained from a single measurement (Fig. 6). The noise level of these parameters is essentially consistent with hysteresis values. The I_S–T curve is essentially consistent with the Is–T curve obtained during the first run (Fig. 5), although Tc = 320 °C (or transition temperature) is unclear in the cooling curve. The heating curve of coercivity (H_C–T) shows a gradual, irregular decrease at temperatures up to ~400 °C before smoothly decreasing and then finally vanishing at around 570 °C. In the cooling curve, H_C appeared from 600 °C, and a remarkable coercivity hump was obtained between 370 and 230 °C (peak at 320 °C). The χ_i–T curve shows a complicated pattern in the heating curve between room temperature and 370 °C. A χ_i peak is observed at ~350 °C in the heating and cooling curves, and at ~260 °C in the cooling curve only. The χ_i value fell to very low values at around 540 °C in the heating curve and was not measurable at 580 °C, whereas it had already started to increase at 600 °C in the cooling curve. The I_R–T curve shows irregular variations up to 350 °C in the heating curve and a small discontinuity at ~300 °C in the cooling curve. The I_R

value approaches zero at 540 °C in the heating curve, and increases again at ~580 °C during cooling.

MICROSCOPIC OBSERVATIONS

A polished thin section of sample C was prepared, for which the distorted layer was removed from the surface by polishing using silica colloidal liquid (<0.1 μm in diameter) (Soffel et al. 1971; Hoffmann et al. 1987). The sample was observed on a reflected light microscope under normal and polarized light and the magnetotactic bacteria (MTB) technique. For this purpose, the horizontal component of the magnetic field at the microscope stage was maintained at <4 μT using Helmholtz coils. Coccus-type MTB of about 1 μm in diameter were cultivated in a 250 cc transparent glass bottle containing a natural medium of sludge and water (Funaki et al. 1989). The MTB living in the northern magnetic hemisphere are expected to migrate to the magnetic S pole along the magnetic field lines. For observations using the optical microscope, a droplet of water containing MTB was placed on the surface of the polished sample using a pipette.

Several ferrimagnetic grains of iron oxide and iron sulfide were analyzed by magneto-force microscope (MFM; Seiko Electric Co., SPA 300 using 20 N of Co-coated cantilever) at 50 nm above the surface to identify the fine magnetic structures. This instrument enables the user to simultaneously capture a topographic image by atomic force microscopy (AMF) and a magnetic image by MFM.

Prior to the MFM experiments, the MTB technique was applied to the polished sample to identify the likely carriers of NRM. As no large clusters or systematic alignments of MTB appeared on the surfaces of the ferrimagnetic grains, the sample was magnetized artificially using a hand magnet (fields of ~0.5 T) to produce an IRM (isothermal remanent magnetization) with S poles on the surface. In this way, representative magnetic grains of iron oxide and iron sulfide were investigated in detail.

Figure 7A shows a backscatter image of large magnetite grain of about 300 × 100 μm in size taken by an electron probe microanalyzer (JXA-8800). Parallel straight lines appeared throughout the grain as well as irregular cracks. When MTB were applied to the grain (Fig. 7B), the densest cluster of bacteria appeared on the lower-left side (as seen in the figure); subsequently, stronger and weaker clusters formed at the center and upper-right, respectively, suggesting the existence of S pole magnetization on the observed surface. Silicate veins, likely representing infilled cracks, were observed at high magnification under normal light (Fig. 7C). Ilmenite exsolution lamellae of <4 μm in width were clearly recognized under cross-polarized light (Fig. 7D).

The rectangular area denoted in Fig. 7C was selected for AFM/MFM experiments. The topography of the surface, as obtained by AFM (Fig. 7E), shows a convex topography for ilmenite and a concave topography for silicate on the magnetite surface due to differences in hardness against mechanical polishing. Complex magnetic domain structures appeared on the magnetite grain (Fig. 7F), with dark (bright) areas representing N (S) magnetization. These magnetic domains are cut by ilmenite laths and silicate veins (cracks) at intervals of ~20 μm. Figures 7G and 7H show AFM and MFM images, respectively, of the area indicated by the rectangular in Fig. 7F. A parallel domain pattern (2–2.5 μm in width) is apparent at the bottom of Figs. 7F and 7H, ultimately revealing the typical structures (180° domain walls) observed on the [110] crystallographic plane of magnetite. Along the silicate vein (or crack) in Fig. 7G, a magnetic field was irradiated resulting from the N and S poles, as indicated by the strong brightness contrasts apparent in Fig. 7H. Analyses by optical microscopy and MFM revealed no low-temperature oxidation (γFe_2O_3) in the investigated grains.

Figure 8A shows an iron sulfide grain of about 40 × 40 μm in size. Part of the grain (upper left in the figure) is replaced by magnetite (this feature might also be an intergrowth), and silicate veins are observed, probably having developed along pre-existing cracks. When MTB were applied to the artificially magnetized surface by IRM, dense clusters appeared on the magnetite portion and parts of the iron sulfide (Fig. 8B), suggesting S pole magnetization at these clusters. An AMF image of the area represented by the square in Fig. 8B reveals a convex topography for iron sulfide and concave topography for silicate veins (Fig. 8C). The MFM pattern obtained for this area (Fig. 8D) yields complicated domain structures of about 1 μm in width in the lower half and right-hand side of the grain. The locations of bacterial clusters largely coincide with the complicated domains, especially on the bright (S poles) areas in the figure. The center of the grain shown in Fig. 8D is probably not magnetized (non-magnetic iron sulfide). In summary, part of the iron sulfide consists of ferrimagnetic, monoclinic pyrrhotite, ($Fe_{1-x}S$; x = 0 to 0.2), with the remainder possibly being non-magnetic pyrrhotite or pentlandite. Microscopic observations reveal that the concentration of iron sulfide is much lower (probably less than 0.05% by volume) than that of magnetite.

Figure 7E shows an area dominated by silicate phases such as augite, olivine, and mesostasis. Numerous fine-grained particles of magnetite (about 10 μm in size) are distributed throughout the mesostasis, as also reported by Imae et al. (2003, 2005); larger grains (>20 μm) occur in mesostasis at the bottom-center part of the figure. When the MTB technique was applied to this artificially magnetized area (IRM), we observed large, small, dense and weak clusters of MTB scattered throughout the mesostasis. As many of the clusters were not overlaid on the magnetite grains visible in Fig. 7E, we inferred that buried or tiny (less than submicron-size) magnetic grains occur below these clusters. Several clusters of MTB also appeared on the augite and olivine grains, suggesting a minor contribution to NRM.

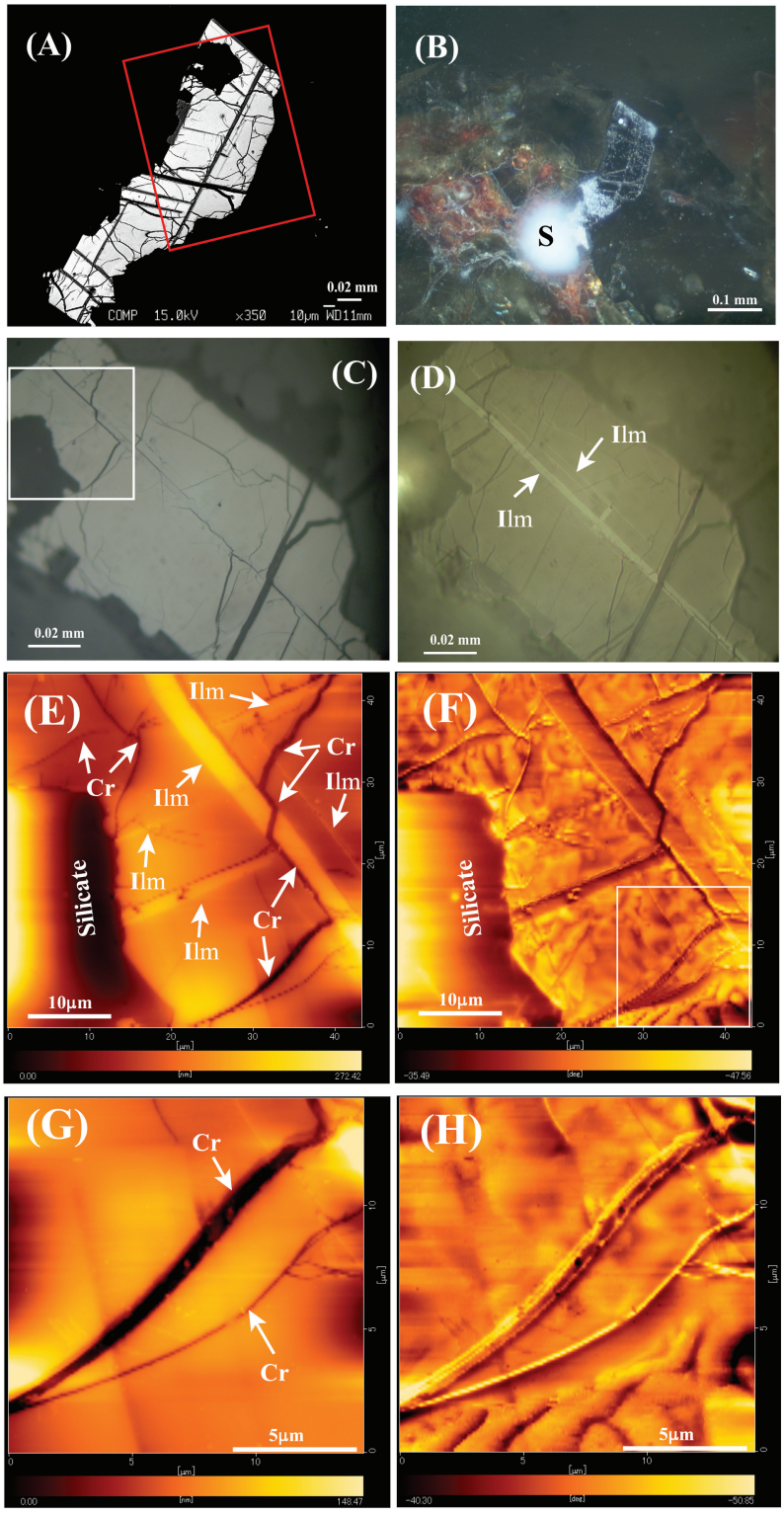

Fig. 7. Magnetic microstructures of a magnetite grain observed under backscatter image (A) of an electron probe microanalyzer, a reflected-light microscope (B–D) and magneto-force microscope (MFM) (topography: E and G; magnetic domain structures: F and H). A) normal light view; B) clusters of magnetotactic bacteria (MTB); C) enlargement of the area outlined by the rectangle in (A); D) polarized light image of the area shown in (C); E) topography of the area outlined by the square in (C); F) magnetic domain structure in the area shown in (E); G) topography (AFM) of the area outlined by the square in (F); H) magnetic domain structure (MFM) in the area shown in (G). Ilm: ilmenite lamellae, Cr: crack or vein, S: magnetized to the S pole.

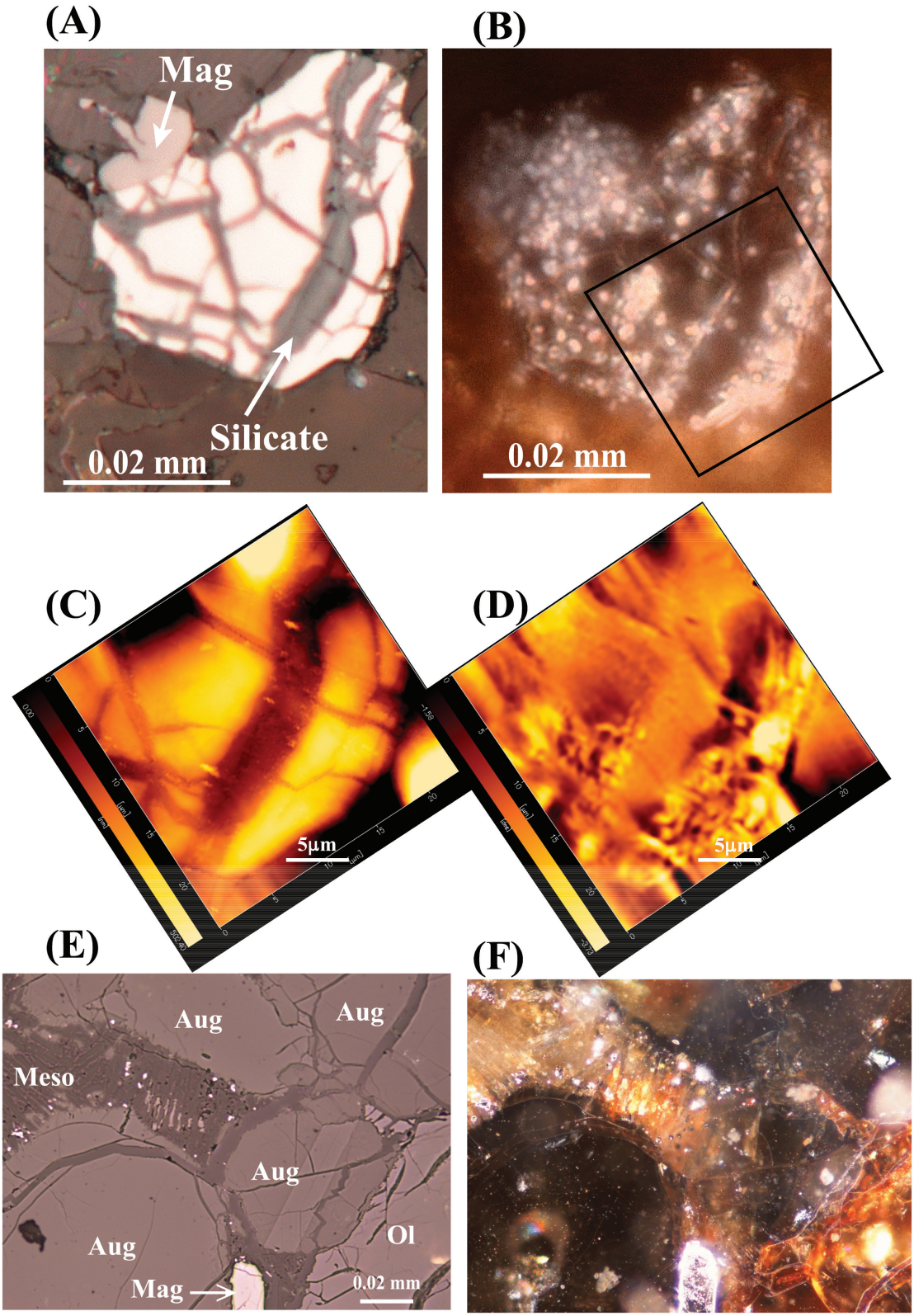

Fig. 8. Magnetic structures of an iron sulfide grain A–D and a silicate-dominated area E and F, as viewed under a reflected light microscope (A), (B), (E), (F) and a magneto-force microscope (topography (C) and domain structure (D). MTB pattern (B) and (F). Mag: magnetite, Aug: augite, Ol: olivine, Meso: mesostasis.

The presence of submicron size of magnetic particles in silicate may provide an explanation for this feature (Hoffmann et al. 2008). A dense cluster of MTB was also observed on the larger magnetite grain located at the bottom-center of the figure.

DISCUSSION

Magnetic Minerals

Imae et al. (2003) reported that the most common opaque mineral in Y-000593 is titanomagnetite (smaller than 0.1 mm, <1 vol%), which is a mixture of magnetite and ulvöspinel that occurs as subhedral to anhedral phenocrysts, usually including ilmenite exsolution lamellae of ~10 μm in width. Abundant, small (~10 μm) titanomagnetite grains are present in the mesostasis. Mikouchi et al. (2003) reported that the (titano-) magnetite contains 1–3 wt% Al_2O_3 and 13–18 wt% TiO_2. Olivine contains symplectic inclusions of magnetite (several microns in size). Small amounts of pyrrhotite ($Fe_{0.86–0.88}S$; <20 μm in diameter) have been detected, especially in the mesostasis (Imae et al. 2003, 2005); however, Mikouchi et al. (2003) identified these grains as pyrite rather than pyrrhotite based on chemical composition. Our results confirm the presence of monoclinic pyrrhotite, at least in the larger sulfide grains in Y-000593.

Based on MTB and MFM observations (Figs. 7 and 8), the magnetic minerals in Y-000593 are confirmed to be (low-Ti) magnetite and monoclinic pyrrhotite. The main Curie point in the heating curve of the first run (Tc = 540 °C) corresponds to (low-Ti) magnetite containing ~5% ulvöspinel (Fe_2TiO_4). The Is value of magnetite containing ~5% ulvöspinel is ~93 Am^2/kg at 0 K (Akimoto 1962). Given that the Is value of Y-000593 is 0.64 Am^2/kg, the amount of magnetite in the sample is calculated to be ~0.68 wt%. The Is value of pyrrhotite is 17.3 Am^2/kg at 0 K, and its Curie point is ~325 °C; however, there exists no evidence of a pyrrhotite Curie point in the I_S–T heating curve of the first run. As the noise level of VSM is less than 1% of the full scale of magnetization (0.012 Am^2/kg in the case of this sample), the concentration of pyrrhotite in the sample is estimated to be less than 0.069 wt%. This estimate, based on the magnetic signature, is consistent with the results of a bulk chemical analysis of Y-000593 (Imae et al. 2003), which found an FeS concentration of 0.07 wt%.

The first run cycle in Fig. 5 yielded an irreversible I_S–T curve with a Curie point shift from Tc = ~540 to 600 °C, suggesting that a thermally stable magnetic mineral (with Tc = 600 °C) formed during heating up to 800 °C under vacuum. The absence of Tc = ~540 °C after the first run heating might reflect superposition of the magnetization of magnetite (Tc = 580 °C) and this unknown phase (Tc = 600 °C). The oscillatory nature of the H_C, I_R, and χ_i curves during heating up to 400 °C in the first run (Fig. 6) may have resulted from this newly produced and altered metastable magnetic mineral(s). The concave shape of the I_S–T cooling curve of the first run (Fig. 5) and the coercivity peak in the H_C–T cooling curve (Fig. 6) between 370 and 230 °C (peak at ~320 °C) suggests the formation of another magnetic phase, possibly a thermally metastable iron oxide (as indicated by the diminishing trend of this likely phase in the second run cycle). Although it could correspond to the formation of monoclinic pyrrhotite by the transformations of hexagonal pyrrhotite or troilite during heating cycle (Rochette et al. 2005), this possibility may be negligible because of too small concentration of iron sulfide in the sample.

Imae et al. (2003) discussed the pre-terrestrial and terrestrial alteration of this meteorite, as indicated by the presence of iddingsite (consisting mainly of goethite (αFeO(OH)) and montmorillonite, $(Na,Ca)_{0.33}(Al,Mg)_2(Si_4O_{10})(OH)_2 \cdot nH_2O$, with both occurring in olivine phenocrysts as reddish-brown veins and dark reddish-brown to black rims). If the iddingsite is of terrestrial origin, it would be less than 0.04 Ma in age, which is the terrestrial age of Y-000593, based on ^{21}Ne analyses (Okazaki et al. 2003). The minor magnetization related to Tc = 75 °C (or transition temperature) in the I_S–T heating curve is well explained by a small amount of goethite, which is also possibly responsible for the unstable behavior (up to 400 °C) in the temperature dependence of the hysteresis parameters. As Lorand et al. (2005) described goethite veins in sulfide grains of SNC meteorites, the veins in the iron oxide and iron sulfide of Y000593 are possibly filled with goethite as well as silicate. In summary, the dominant magnetic mineral within the Y-000593 nakhlite is magnetite (low-Ti titanomagnetite), with monoclinic pyrrhotite and goethite possibly present at lower, perhaps even negligible concentrations.

Significance of NRM

The NRM of Y-000593 was extremely unstable against AF demagnetization, although the intensity ($R = 3.55–6.07 \times 10^{-5}$ Am^2/kg) is similar to that of other nakhlites ($1.3–7.92 \times 10^{-5}$ Am^2/kg), as shown in Table 1. Low REM value of 5.5×10^{-4} (Table 1) yields that the NRM was not contaminated magnetically by an artificial magnet, etc.: REM = $\sim10^{-2}$ for volcanic rocks and REM = $\sim10^{-3}$ for extrusive and metamorphic rocks (Cisowski et al. 1990). This low value is classified into the lowest group of the REM values among Martian meteorites (Rochette, et al. 2001; Gattacceca and Rochette, 2004): dominant REM values are in the range of $2.6 \times 10^{-4} – 7.9 \times 10^{-3}$. The ARM coercivity spectra (Fig. 3) suggest that Y000593 takes a potential ability to carry the stable NRM at least 55 mT. Although the NRM was thermally demagnetized at ~330 °C, coinciding with the Curie point of monoclinic pyrrhotite, the low concentration of pyrrhotite in the sample (less than 0.069 wt%) indicates that the NRM is carried by MD magnetite grains. The demagnetization might be yielded due to an offset of the antipodal magnetizations as

observed at 280 and 380 °C. Based on these observations, we conclude that the NRM of Y-000593 was acquired as IRM or a viscous remanent magnetization (VRM), most likely in the terrestrial magnetic field; however, Y-000593 has the ability to record a stable remanent magnetization, as numerous SD and PSD magnetite grains (<10 μm) are scattered throughout the silicate mineral phases, especially the mesostasis. The large MD magnetite grains contain ilmenite (exsolution) lamellae, silicate (including goethite) veins, and/or cracks at intervals of ~20 μm. These structures might have enhanced the stability of the NRM. The moderate coercivities (H_C = 6.8 mT and H_{RC} = 31.1 mT) and the coercivity spectra of ARM up to 55 mT support the ability to carry stable NRM, based on the results of analyses of terrestrial basalt (e.g., Funaki 1983).

Estimation of the Magnetic Field on Mars

Despite the presence of numerous SD and PSD magnetite grains in the mesostasis, Y-000593 does not carry any significant NRM components, suggesting no external magnetic field when Y00593 was crystallized in Mars. If it carries a significant NRM component of Martian origin, the precision of the paleointensity obtained by Thellier and Thellier (1959) method seems to be 0.1 μT based on our laboratory experiences. This may suggest that external magnetic field was extremely weak or absent during the formation of this meteorite. One hypothesis to consider is that the meteorite did not acquire any TRM below 540 °C during the cooling stage of crystallization because of the absence of an external magnetic field in the required temperature range. The crystallization age of Y-000593 is 1.31 ± 0.03 Ga based on Sm-Nd isochron (Shih et al. 2002), 1.269 ± 0.24 Ga based on Rb-Sr (Nakamura et al. 2002) and 1.30 ± 0.02 Ga based on Rb-Sr dating (Misawa et al. 2005). One possibility is that the magnetic field on Mars fell into decay at 1.3 Ga, or was only weakly developed. A second plausible possibility is shock demagnetization (e.g., Pohl et al. 1975; Cisowski et al. 1978), whereby the impactite is first demagnetized and then remagnetized in the direction of the external magnetic field at shock values higher than 0.1 GPa. If an external magnetic field does not exist at the time of the shock event, any stable NRM may be absent due to shock demagnetization. In contrast, Funaki and Syono (2008) demonstrated that the scattered directions of remanent magnetization resulting from shock remagnetization in the external magnetic field of 7 μT are characteristic of shocks between 5 and 20 GPa. Therefore, analyses of the shock demagnetization and remagnetization processes of Martian meteorites are of major importance in understanding the results of paleomagnetic studies. Based on micro-Raman spectroscopy, Fritz et al. (2005) reported shock pressures above 40 GPa for Martian meteorites, although generally less than 20 GPa for the nakhlites (including Y-000593). The cracks and veins observed throughout the larger magnetite and sulfide grains in the analyzed sample are typical shock features of Y-000593. The silicate (goethite)-filled cracks possibly formed before the time of ejection from Mars, as hydrothermal activity in the parent body appears to have transferred silicate and goethite materials into the cracks. Given that Okazaki et al. (2003) reported an ejection time from Mars of 12.1 ± 0.7 Ma for Y-000593, based on ^{21}Ne exposure, the severe shock possibly occurred between the crystallization age (1.3 Ga) and the time of ejection, with hydrothermal activity occurring subsequent to the shock. The shock that occurred at the time of ejection was probably relatively weak, because the rock at this stage was soft, brittle, and of low density (2.20 ± 0.04 g/cc); it is therefore possible that severe shock waves did not reach the analyzed sample because of large shock impedance. Given the scenario of shock demagnetization in case of Y-00593, the magnetic field of Mars must have been absent at that severe shock.

Previous studies have used various techniques to estimate paleomagnetic field intensities during the formation of SNC meteorites on Mars. The intensities were found to be lower than the present geomagnetic field, and different intensities were obtained from the same SNC meteorite by different researchers, as follows: 0.25–2.0 μT for Shergotty analyzed by Cisowski (1986); 1.0 μT for ALHA77005 analyzed by Cisowski (1986), but only a VRM was obtained by Collinson (1986); 4.0 μT for Nakhla analyzed by Shaw et al. (2001) and 0.7–3.2 μT analyzed by Collinson (1997), but inconclusive results were obtained by Cisowski (1986); and 1.0–10.0 μT for EETA79001 analyzed by Collinson (1986) and 0.8–3.6 μT by Collinson (1997), but again inconclusive results as described the weak magnetic field were obtained by Cisowski (1986). Collinson (1997) reported paleointensity values of 0.5–5.0 μT for Governador Valadares, Zagami, Lafayette, and Chassigny. In the case of ALH 84001, Weiss et al. (2002) obtained ~50 μT; however, Cisowski (1986) failed to obtain reasonable values, and Kirschvink et al. (1997) reported scattered NRMs. Cisowski (1986) failed to obtain clear paleointensity values in analyses of Zagami and Governador Valdares. Rochette et al. (2001, 2005) proposed that the very low thermal stability of magnetic remanence in some SNCs is due to the presence of hexagonal pyrrhotite in a metastable ferrimagnetic state or shock-induced substructures in monoclinic pyrrhotite. Given that magnetite is the dominant NRM carrier in Y-000593, this problem related to pyrrhotite is of negligible concern in the present study. Therefore, the results of our investigations of NRM behavior in the nakhlite Y-000593 provide the first clear evidence of an extremely weak or non-existent magnetic field between 1.3 Ga (formation age) and 12 Ma (ejection age) on Mars. Namely, the significant dipole magnetic field resulting from the molten metallic core might have been absent during the Amazonian Epoch (after 1.8 Ga) on Mars, although the magnetic field resulting from a dynamo was widely accepted in the early stage of Mars (e.g. Connerney et al. 2001).

CONCLUSION

The dominant magnetic mineral in Y-000593 is low-Ti magnetite (0.68 wt%), along with minor monoclinic pyrrhotite and goethite. Homogeneous titanomagnetite grains have yet to be observed in nakhlites, including Y-000593; however, ilmenite exsolution lamellae are common, as are silicate (including goethite) -filled cracks spaced at intervals of ~20 μm. Relatively uniform NRM intensities ($3.55–6.07 \times 10^{-5}$ Am^2/kg) in Y-000593 are similar to those in other nakhlites (Nakhla and Governador Valdares). The NRM is unstable against AF demagnetization; however, Y-000593 is physically able to carry stable magnetic remanences, as indicated by its grain size and coercivity values. Although the NRM was demagnetized at ~320 °C (similar to the Curie point of monoclinic pyrrhotite), it was most likely carried only by MD magnetite (including ~5% Fe_2TiO_4). The concentrations of magnetite and pyrrhotite in Y-000593 are estimated to be 0.68 wt% and <0.069 wt%, respectively. We propose two plausible explanations of the unstable NRM behavior: the external magnetic field on Mars was extremely weak or absent (1) when the meteorite was crystallized at 1.3 Ga (no acquisition of TRM) or (2) when the meteorite was demagnetized by shock between 1.3 Ga and the ejection time (12.1 ± 0.7 Ma). Probably the molten metallic core to produce the dipole magnetic field might have been absent during the Amazonian Epoch (after 1.8 Ga) on Mars.

Acknowledgments—The authors wish to thank Prof. R. B. Scorzelli (Centro Brasileiro de Pesquisas Fisicas, Brazil) and Prof. M. Torii (Okayama University of Science, Japan) for discussions of magnetic minerals in Y-000593.

Editorial Handling—Dr. Allan Treiman

REFERENCES

Akimoto S. 1962. Magnetic properties of FeO-Fe_2O_3-TiO_2 system as a basic of rock magnetism. *Journal of the Physical Society of Japan* 17(B1):706–710.

Cisowski S. M., Dunn J. R., Fuller M., and Wasilewski P. J. 1990. NRM:IRM(s) demagnetization plots of intrusive rocks and the origin of their NRM. *Tectonophysics* 184:35–54.

Cisowski S. M. 1986. Magnetic studies on Shergotty and other SNC meteorites. *Geochimica et Cosmochimica Acta* 50: 1043–1048.

Cisowski S. M. and Fuller M. 1978. The effect of shock on the magnetism of terrestrial rocks. *Journal of Geophysical Research* 83(B7):3441–3458.

Collinson D. W. 1986. Magnetic properties of Antarctic shergottite meteorites EETA79001 and ALHA77005: possible relevance to a Martian magnetic field. *Earth and Planetary Science Letters* 77:159–164.

Collinson D. W. 1997. Magnetic properties of Martian meteorites: Implications for an ancient Martian field. *Meteoritics & Planetary Science* 32:803–811.

Connerney J. E. P., Acuña M. H., Wasilewski P. J., and Kleteschka G. 2001. The global magnetic field of Mars and implications for crustal evolution. *Geophysical Research Letters* 28(21):4015–4018.

Day R. 1977. TRM and its variation with grain size. *Journal of Geomagnetism and Geoelectricity* 29:233–265.

Fritz J., Greshake A., and Stöffler D. 2005. Micro-Raman spectroscopy of plagioclase and maskelynite in Martian meteorites: Evidence of progressive shock metamorphism. *Antarctic Meteorite Research* 18:96–116.

Funaki M. 1983. Paleomagnetic investigation of McMurdo Volcanics, Antarctica. *Nankyoku Shiryo (Antarct. Rec.)* 77:1–19.

Funaki M. and Syono Y. 2008, Acquisition of shock remanent magnetization for demagnetized samples in a weak magnetic field (7 μT) by shock pressures 5–20 GPa without plasma induced. *Meteoritics & Planetary Science* 43:529–240.

Funaki M., Sakai H., and Matsunaga, T. 1989. Identification of the magnetic poles on strong magnetic grains from meteorites using magnetotactic bacteria. *Journal of Geomagnetism and Geoelectricity* 41:77–87.

Gattacceca J. and Rochette P. 2004. Toward a robust normalized magnetic paleointensity method applied to meteorites. *Earth and Planetary Science Letters* 227:377–393.

Hoffmann V., Funaki M., and Torii M., Hochleitner R., and Classen N. 2008. Systematic survey on the magnetic signature of Martian meteorites (SNC): Extending the database (abstract). *Meteoritics & Planetary Science* 43:A59.

Hoffmann V., Schäfer R., Appel E., Hubert A., and Soffel H. C. 1987. First domain observations with magneto-optical Kerr effect on titan-ferrites in rocks and their synthetic equivalents. *Journal of Magnetism and Magnetic Materials* 71:90–94.

Imae N., Ikeda Y., Kojima H., and Iwata N. 2003. Yamato nakhlites: petrography and mineralogy. *Antarctic Meteorite Research* 16: 13–33.

Imae N., Ikeda Y., and Kojima H. 2005. Petrology of Yamato nakhlites. *Meteoritics & Planetary Science* 40:1581–1598.

Kirschvink J. L., Maine A. T., and Vail H. 1997. Paleomagnetic evidence of a low-temperature origin of carbonate in the Martian meteorite ALH 84001. *Science* 275:1629–1633.

Koenigsberger J. G. 1938. Natural residual magnetism of eruptive rocks. *Terrestrial Magnetism and Atmospheric Electricity* 43: 119–130.

Lorand J. P., Chevrier V., and Sautter V. 2005. Sulfide mineralogy and redox conditions in some shergottites. *Meteoritics & Planetary Science* 40:1257–1272.

McSween H. Y. Jr. 1985. SNC meteorites: Clues to Martian petrologic evolution? *Reviews of Geophysics* 23:391–416.

Mikouchi T., Koizumi E., Monkawa A., Ueda T., and Miyamoto M. 2003. Mineralogy and petrology of Yamato 000593: Comparison with other Martian nakhlite meteorites. *Antarctic Meteorite Research* 16:34–57.

Misawa K., Shih C., Wiesmann H., and Garrison D. H. 2005. Rb-Sr, Sm-Nd and Ar-Ar isotopic systematics of Antarctic nakhlite Yamato 000593. *Antarctic Meteorite Research* 18:133–151.

Nakamura N., Yamakawa A., Yamashita K., Kobayashi T., Imae N., Misawa K., and Kojima H. 2002. Ree abundances and Rb-Sr age of a new Antarctic nakhlite Yamato 000593. 27th Symposium on Antarctic Meteorites. pp. 112–114.

Okazaki R., Nagao K., Imae N., and Kojima H. 2003. Nobel gas signatures of Antarctic nakhlites, Yamato (Y) 000593, Y000749, and Y000802. *Antarctic Meteorite Research* 16:58–79.

Pohl J., Bleil U., and Hornemann U. 1975. Shock magnetization and demagnetization of basalt by transient stress up to 10 kbar. *Journal of Geophysics* 41:23–41.

Rochette P., Lorand J., Fillion G., and Sautter V. 2001. Pyrrhotite and

the remanent magnetization of SNC meteorites: A changing perspective on Martian magnetism. *Earth and Planetary Science Letters* 190:1–12.

Rochette P., Gattacceca J., Chevrier V., Hoffmann V., Lorand J. P., Funaki M., and Hochleitner R. 2005. Matching Martian crustal magnetization and meteorite magnetic properties. *Meteoritics & Planetary Science* 40:529–540.

Shaw J., Hill M. J., and Openshaw S. J. 2001. Investigating the ancient Martian magnetic field using microwaves. *Earth and Planetary Science Letters* 190:103–109.

Shih C. Y., Wiesmann H., Nyquist L. E., and Misawa K. 2002. Crystallization age of Antarctic nakhlite Y000593 (abstract). 27th Symposium on Antarctic Meteorites. pp. 151–153.

Soffel H. and Petersen N. 1971. Ionic etching of titanomagnetite grains in basalts. *Earth and Planetary Science Letters* 11:312–316.

Thellier E. and Thellier O. 1959. Sur I'intensite du champ magnétique terrestre dans le passé historique et géologique. *Annales de Geophysique* 15:285–376.

Weiss B. P., Vali H., Baudenbacher F. J., Kirschvink J. L., Stewart S. T., and Shuster D. L. 2002. Records of an ancient Martian magnetic field in ALH 84001. *Earth and Planetary Science Letters* 201:449–463.